Seawater redox variations during the deposition of the Kimmeridge Clay Formation, United Kingdom (Upper Jurassic): Evidence from molybdenum isotopes and trace metal ratios

Christopher R. Pearce,[1] Angela L. Coe,[1] and Anthony S. Cohen[1]

Received 22 March 2010; revised 16 July 2010; accepted 23 July 2010; published 12 November 2010.

[1] The Kimmeridge Clay Formation (KCF) and its equivalents worldwide represent one of the most prolonged periods of organic carbon accumulation of the Mesozoic. In this study, we use the molybdenum (Mo) stable isotope system in conjunction with a range of trace metal paleoredox proxies to assess how seawater redox varied both locally and globally during the deposition of the KCF. Facies with lower organic carbon contents (TOC 1–7 wt %) were deposited under mildly reducing (suboxic) conditions, while organic-rich facies (TOC >7 wt %) accumulated under more strongly reducing (anoxic or euxinic) local conditions. Trace metal abundances are closely linked to TOC content, suggesting that the intensity of reducing conditions varied repeatedly during the deposition of the KCF and may have been related to orbitally controlled climate changes. Long-term variations in $\delta^{98/95}$Mo are associated with the formation of organic-rich intervals and are related to third-order fluctuations in relative sea level. Differences in the mean $\delta^{98/95}$Mo composition of the organic-rich intervals suggest that the global distribution of reducing conditions was more extensive during the deposition of the *Pectinatites wheatleyensis* and lower *Pectinatites hudlestoni* zones than during the deposition of the upper *Pectinatites hudlestoni* and *Pectinatites pectinatus* zones. The global extent of reducing conditions during the Kimmerigidan was greater than today but was less widespread than during the Toarcian (Early Jurassic) oceanic anoxic event. This study also demonstrates that the Mo isotope system in Jurassic seawater responded to changes in redox conditions in a manner consistent with its behavior in present-day sedimentary environments.

Citation: Pearce, C. R., A. L. Coe, and A. S. Cohen (2010), Seawater redox variations during the deposition of the Kimmeridge Clay Formation, United Kingdom (Upper Jurassic): Evidence from molybdenum isotopes and trace metal ratios, *Paleoceanography*, *25*, PA4213, doi:10.1029/2010PA001963.

1. Introduction

1.1. Geological Setting and Stratigraphy

[2] The Kimmeridge Clay Formation (KCF) was deposited across much of Northern Europe between ~155 and ~148 Ma during the Late Jurassic Kimmeridgian Age *sensu anglico* (equivalent to the Kimmeridgian *sensu gallico* and early Tithonian) [*Gradstein et al.*, 2004]. As such, it represents one of the most prolonged periods of organic carbon accumulation to have occurred during the Mesozoic [*Hallam*, 1987; *Jenkyns et al.*, 2002], and the formation now acts as a major petroleum source rock [*Glennie*, 1998]. Sedimentary rocks with total organic carbon (TOC) contents of <2 wt % to >50 wt % (averaging 4.2 wt %) [*Coe*, 1992; *Tyson*, 2004] were deposited in a series of shallow marine basins in the epicontinental Laurasian Seaway. This N-S trending seaway connected the Boreal and Tethyan oceans and was associated with low-lying islands of various sizes scattered throughout the region (Figure 1) [*Smith et al.*, 1994; *Ziegler*, 1990]. Ammonites from the Kimmeridgian deposits of this region suggest that the surface currents flowed southward from the Boreal Ocean and overlay warmer saline bottom waters produced in the Tethyan Ocean [*Miller*, 1990].

[3] The type section of the KCF, exposed along the Dorset coast, United Kingdom, accumulated near the main depocenter of the Wessex Basin and reaches a maximum thickness of ~550 m [*Cox and Gallois*, 1981]. The different parts of the section are usually referred to by the 13 ammonite zones into which it is divided [*Cope et al.*, 1980]. The type section contains five bands particularly rich in organic matter that are tens of meters thick and have been referred to as organic-rich intervals (ORIs) [*Herbin et al.*, 1995; *Jenkyns et al.*, 2002, *Tribovillard et al.*, 2004b]. These ORIs, which are also present in contemporaneous Kimmeridgian deposits in the Cleveland Basin, Yorkshire, and the Boulonnais region of northern France, occur in the middle of the *Aulacostephanus eudoxus* zone, the upper *eudoxus* to lower *Aulacostephanus autissodorensis* zones, the *Pectinatites elegans* to lower *Pectinatites scitulus* zones, the upper *Pectinatites wheatleyensis* to lower *Pectinatites hudlestoni* zones, and the upper *hudlestoni* to lower *Pectinatites pectinatus* zones (Figure 2). In addition to high TOC, the ORIs are also associated with increases in $\delta^{13}C_{org}$ that are interpreted to reflect the enhanced burial of isotopically light organic carbon within the marine

[1]Department of Earth and Environmental Sciences, Centre for Earth, Planetary, Space and Astronomical Research, Open University, Walton Hall, Milton Keynes, UK.

0883-8305/10/2010PA001963

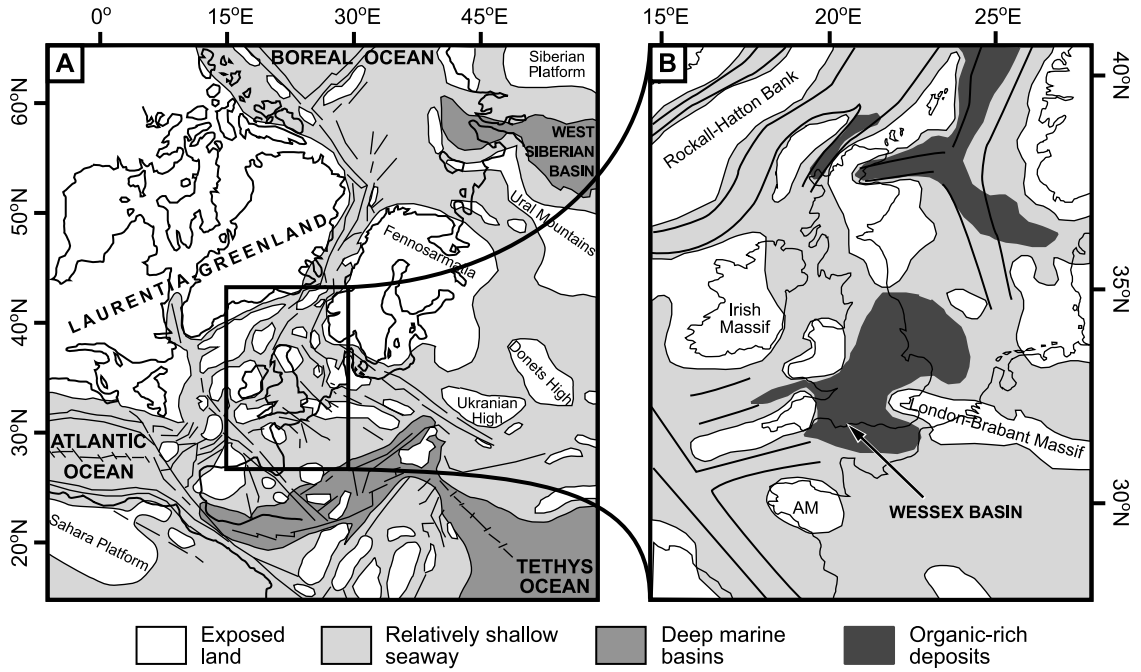

Figure 1. (a) Kimmeridgian palaeogeography of the Laurasian Seaway and northwest Europe, adapted from the compilation of *Chambers et al.* [2000]. (b) The inferred extent of organic-rich sediment accumulation during the early Kimmeridgian *eudoxus* zone, showing the location of the Kimmeridge type section in the Wessex Basin [after *Oschmann*, 1988, 1990]. AM, Amorcian Massif.

basins [*Jenkyns et al.*, 2002; *Morgans-Bell et al.*, 2001]. The highest $\delta^{13}C_{org}$ values of ~−21‰ occur within the Blackstone Band of the *wheatleyensis* zone, which is one of the most organic-rich horizons in the KCF with a TOC content of up to 50 wt % (Figure 2) [*Coe*, 1992; *Morgans-Bell et al.*, 2001; *Tyson*, 2004]. The first ORI (in the mid-*eudoxus* zone) is also associated with a positive shift in $\delta^{13}C_{carb}$, seen in records from hemipelagic carbonates deposited in the northern Tethys [*Padden et al.*, 2002; *Weissert and Mohr*, 1996], suggesting that the burial of organic matter at that time might have been sufficiently large so as to affect the carbon cycle further afield. The five ORIs are separated by sedimentary deposits with lower TOC contents (typically 1–7 wt %). These intervals are referred to as the organic-poor intervals (OPIs), even though their organic carbon content is significantly higher than that of an "average" shale [*Piper and Calvert*, 2009; *Tribovillard et al.*, 2004b].

[4] The mudrock facies also vary cyclically on a smaller 1–10 m scale throughout the KCF, reflecting variations in the proportion of clay minerals, TOC and $CaCO_3$. Time series analysis of the variation in magnetic susceptibility, photoelectric factor, and total gamma ray demonstrates that the periodicity of the cycles was controlled by Milankovitch orbital parameters [*Dunn*, 1974; *Huang et al.*, 2010; *Weedon et al.*, 1999, 2004]. This astronomical control on the composition of the KCF has been attributed to changes in both marine productivity and the preservation of organic matter [*Piper and Calvert*, 2009]. Marine productivity would have been enhanced during climatic optimums as a result of higher temperatures and higher pCO_2, resulting in a larger net transfer of organic matter to the sediment-water interface. The preservation of organic matter also depends on the availability of oxygen, with more organic matter being preserved under reducing conditions due to a lower rate of oxidation. The extent to which each mechanism was responsible for the high organic carbon content of the KCF has been discussed extensively in the literature [*Bertrand and Lallier-Vergès*, 1993; *Cox and Gallois*, 1981; *Demaison and Moore*, 1980; *Lallier-Vergès et al.*, 1993, 1997; *Morgans-Bell et al.*, 2001; *Oschmann*, 1988, 1990; *Sælen et al.*, 2000; *Sinninghe Damsté et al.*, 2001; *Tribovillard et al.*, 1994; *Tyson*, 1979, 2005; *van Dongen et al.*, 2006; *van Kaam-Peters et al.*, 1998a, 1998b; *Weedon et al.*, 2004] and is not considered further here.

[5] Most paleoredox information for the availability of O_2 in the depositional environment of the KCF comes from specific intervals [e.g., *Lees et al.*, 2004, 2006; *Pearson et al.*, 2004; *Wignall and Meyers*, 1988]. The identification of isorenieratane in the KCF demonstrates that euxinic conditions (no O_2 and "free" H_2S within the water column) must have extended into the photic zone at various times during the Kimmeridgian [*Sælen et al.*, 2000; *Sinninghe Damsté et al.*, 2001]. Sedimentary rocks in the KCF with TOC <10 wt % contain lower levels of the redox-sensitive trace metals (such as Mo, V, and U) but have a positive correlation with the degree of pyritisation (DOP), while sedimentary rocks with a higher TOC (>10%) have higher concentrations of redox-sensitive trace elements and DOP values >90% that do not covary with TOC [e.g., *Dunn*, 1974; *Tribovillard et al.*, 1994, 2004a, 2004b; *Wignall and Meyers*, 1988]. The covariance between $\delta^{15}N$ and $\delta^{13}C_{TOC}$ in samples from the *wheatleyensis* to *pectinatus* zones is thought to reflect an increase in nitrate

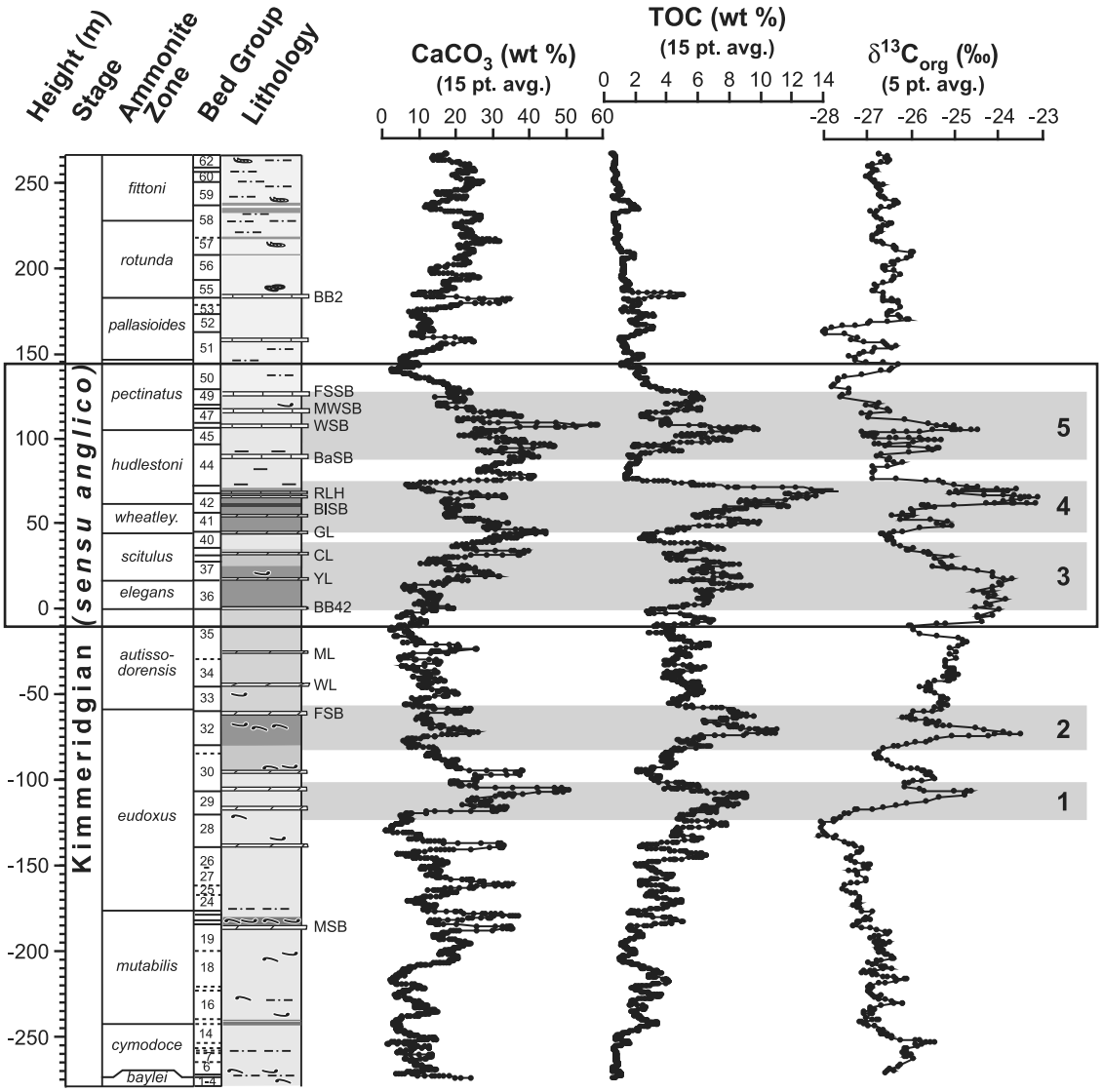

Figure 2. Summary graphic log, biostratigraphy, and chemostratigraphy of the Kimmeridge Clay Formation (KCF) in Dorset, after *Morgans-Bell et al.* [2001]. MSB, Metherhills Stone Band; FSB, Flats Stone Band; WL, Washing Ledge; ML, Maple Ledge; BB42, Blake's Bed 42; YL, Yellow Ledge; CL, Cattle Ledge; GL, Gray Ledge; BlSB, Blackstone Band; RLH, Rope Lake Head; BaSB, Basalt Stone Band; WSB, White Stone Band; MWSB, Middle White Stone; FSSB, Freshwater Steps Stone Band; BB2, Blake's Bed 2. The zero datum height used in this study is the base of Blake's Bed 42, which corresponds to the base of the *elegans* zone. The high-resolution $CaCO_3$, TOC, and $\delta^{13}C$ data were collected as part of the Rapid Global Geological Events (RGGE) project and represent 15-point ($CaCO_3$, TOC) and 5-point ($\delta^{13}C$) moving averages [*Morgans-Bell et al.*, 2001; *Jenkyns et al.*, 2002; *Weedon et al.*, 2004]. The five organic-rich intervals (ORIs) [*Herbin et al.*, 1995; *Jenkyns et al.*, 2002; *Tribovillard et al.*, 2004b] in the KCF are highlighted in gray and numbered sequentially. The box represents the part of the formation that was investigated in this study and includes the last three ORIs.

and/or ammonium utilization by phytoplankton within a suboxic/anoxic water column [*Sælen et al.*, 2000]. Variations in $\delta^{57/54}$Fe indicate that redox-dependent cycling of Fe may have occurred during the *autissodorensis* to *pallasioides* zones, although interpretation of the $\delta^{57/54}$Fe data is complicated by evidence for diffusional Fe-isotope exchange during diagenesis [*Matthews et al.*, 2004]. Taken together, these paleoredox proxies suggest that the redox state of the depositional environment varied considerably in both time and space during the accumulation of the KCF.

1.2. Molybdenum Stable Isotope System

[6] The Mo isotope system has attracted particular attention as a paleoredox proxy because, uniquely, it has the

potential to record changes in the extent of both local and global marine anoxia [*Anbar*, 2004; *Arnold et al.*, 2004; *Pearce et al.*, 2008; *Poulson et al.*, 2006; *Siebert et al.*, 2003]. Molybdenum occurs in present-day seawater predominantly as the chemically inert molybdate ion MoO_4^{2-}, which is slowly removed under oxidizing marine conditions through assimilation into ferromanganese phases and other authigenic material [e.g., *Emerson and Huested*, 1991; *Morford and Emerson*, 1999]. The isotopically light oxic Mo isotope composition ($\delta^{98/95}Mo_{oxic}$ ~−0.6‰) of these phases results from the preferential incorporation of lighter Mo isotopes and causes residual Mo in seawater to be enriched in heavier Mo isotopes ($\delta^{98/95}Mo_{seawater}$ ~2.4‰) [*Barling and Anbar*, 2004; *Pearce et al.*, 2009; *Poulson et al.*, 2006]. The $\delta^{98/95}Mo_{seawater}$ value of the present-day oceans is uniform because the marine residence time of Mo (~800 ka) is considerably greater than the mixing time of the oceans [*Anbar*, 2004]. It also appears that $\delta^{98/95}Mo_{seawater}$ has been constant over the last ~60 Ma [*Siebert et al.*, 2003], at least at the 1–3 Ma resolution over which that study was conducted. Under euxinic conditions, dissolved molybdate is converted quantitatively to MoS_4^{2-} without isotopic fractionation, such that $\delta^{98/95}$Mo in euxinic sedimentary deposits reflects the isotopic composition of Mo in the coeval seawater (i.e., $\delta^{98/95}Mo_{euxinic} \approx \delta^{98/95}Mo_{seawater} \approx 2.4‰$) [*Tossell*, 2005; *Neubert et al.*, 2008; *Poulson et al.*, 2006]. Thus, by measuring the $\delta^{98/95}$Mo value of hydrogenous Mo within euxinic sedimentary deposits, the palaeo $\delta^{98/95}Mo_{seawater}$ value can be determined and used to infer the global proportion of oxic-reducing sedimentation [*Anbar*, 2004; *Arnold et al.*, 2004; *Ling et al.*, 2005; *Pearce et al.*, 2008]. The $\delta^{98/95}$Mo values of sediments deposited in anoxic open-ocean sites today, where $[H_2S]$ is substantially lower then in euxinic settings (i.e., on the continental margins), fall within an intermediate range that is generally close to 1.6‰, while the $\delta^{98/95}$Mo ratios of suboxic sediments (that have low O_2 but no H_2S) are between −0.7‰ and 1.6‰ [*McManus et al.*, 2006; *Poulson et al.*, 2006; *Siebert et al.*, 2006].

[7] The use of the Mo isotope system as a proxy for determining the areal extent of marine anoxia in the past depends on the assumption that the depositional environment was both euxinic and open to the global ocean. One of the most useful geochemical proxies for assessing the redox state of the local depositional environment is the degree of pyritisation (DOP). This parameter reflects how much Fe^{3+} has been reduced to Fe^{2+} and combined with sulfide to form pyrite, which is calculated from the relative amounts of "reactive" and "nonreactive" iron in the sample [*Raiswell and Berner*, 1985; *Raiswell et al.*, 1988]. A good approximation for DOP can be obtained using the total amount of Fe and S present and is based on the assumption that all sulfur in the sediment is present as pyrite. The degree of pyritisation determined in this manner is referred to as DOP_T where

$$DOP_T(\%) = \left(\frac{TS \times 0.86}{TFe}\right) \times 100.$$

[8] Trace metal abundances and abundance ratios are also sensitive to the amount of dissolved oxygen and can therefore also be used as local paleoredox proxies. For example, differences between the redox potentials of Re and Mo cause oxic/suboxic sediments to be preferentially enriched in Re with respect to Mo, whereas both metals are equally enriched in strongly reducing sediments [*Crusius and Thomson*, 2000; *Crusius et al.*, 1996]. Low Re/Mo ratios similar to that of seawater (~0.4 mmol/L in the present-day oceans) [*Crusius et al.*, 1996] consequently suggest that deposition occurred in a strongly reducing environment. *Algeo and Tribovillard* [2009] used the relative enrichments of Mo and U to assess variations in both redox state and basinal restriction within modern and ancient paleoceanographic systems. The enrichment factor (EF) of each element is defined relative to the Post-Archean Average Shale (PAAS) composition as $X_{EF} = [(X/Al)_{sample}/(X/Al)_{PAAS}]$. As with the Re/Mo system, the rate of Mo accumulation increases relative to the rate of U accumulation in sulfidic (euxinic) environments, causing the Mo/U ratio to equal or exceed that of seawater. The relative enrichment of Mo may subsequently decrease within strongly restricted settings owing to limited Mo renewal [*Algeo and Tribovillard*, 2009]. V/Ni ratios can also be used as a paleoredox proxy as Ni is preferentially adsorbed to organic matter and incorporated into pyrite within euxinic sediments. Lower V/Ni ratios therefore indicate enhanced organic carbon burial under strongly anoxic/euxinic conditions, while higher ratios suggest deposition under less reducing environments [e.g., *Tribovillard et al.*, 1994, 2006].

[9] In this study, a range of geochemical paleoredox proxies has been employed to determine both the local depositional environment of the upper part of the KCF (~151 to ~149 Ma) at its type section in Dorset, United Kingdom, and the global redox conditions at that time. Measured $\delta^{95/95}$Mo ratios, Mo abundances, Re/Mo, Mo/U and Vi/Ni ratios, as well as DOP_T have been used in conjunction with changes in TOC and facies type to establish how the redox state of the depositional environment varied between the *autissodorensis* and the *pectinatus* zones. The $\delta^{95/95}$Mo data from the KCF are also compared with those from the organic-rich Whitby Mudstone Formation (WMF), Yorkshire, United Kingdom, which was deposited during the Toarcian (Early Jurassic) OAE [*Pearce et al.*, 2008]. On the basis of this comparison between both organic-rich units, the applicability of the Mo isotope system as a paleoredox proxy is assessed.

2. Materials and Methods

[10] Bulk-rock samples were collected by *Coe* [1992] from the KCF type section exposed on the Dorset coast and were positioned accurately with respect to detailed stratigraphic logs [*Coe*, 1992; *Morgans-Bell et al.*, 2001]. In the present study 39 samples were analyzed from the upper *autissodorensis* to *pectinatus* zones. Cyclostratigraphic dating indicates that these zones were deposited over an interval of ~2.3 Ma (Figure 3) [*Weedon et al.*, 2004], equating to an average sample resolution of ~58 ka. The section studied includes three of the intervals that are particularly enriched in organic carbon (ORIs 3–5), one of which is the extremely organic-rich Blackstone Band where TOC contents reach 50 wt % (Figure 2). Samples were taken from five different

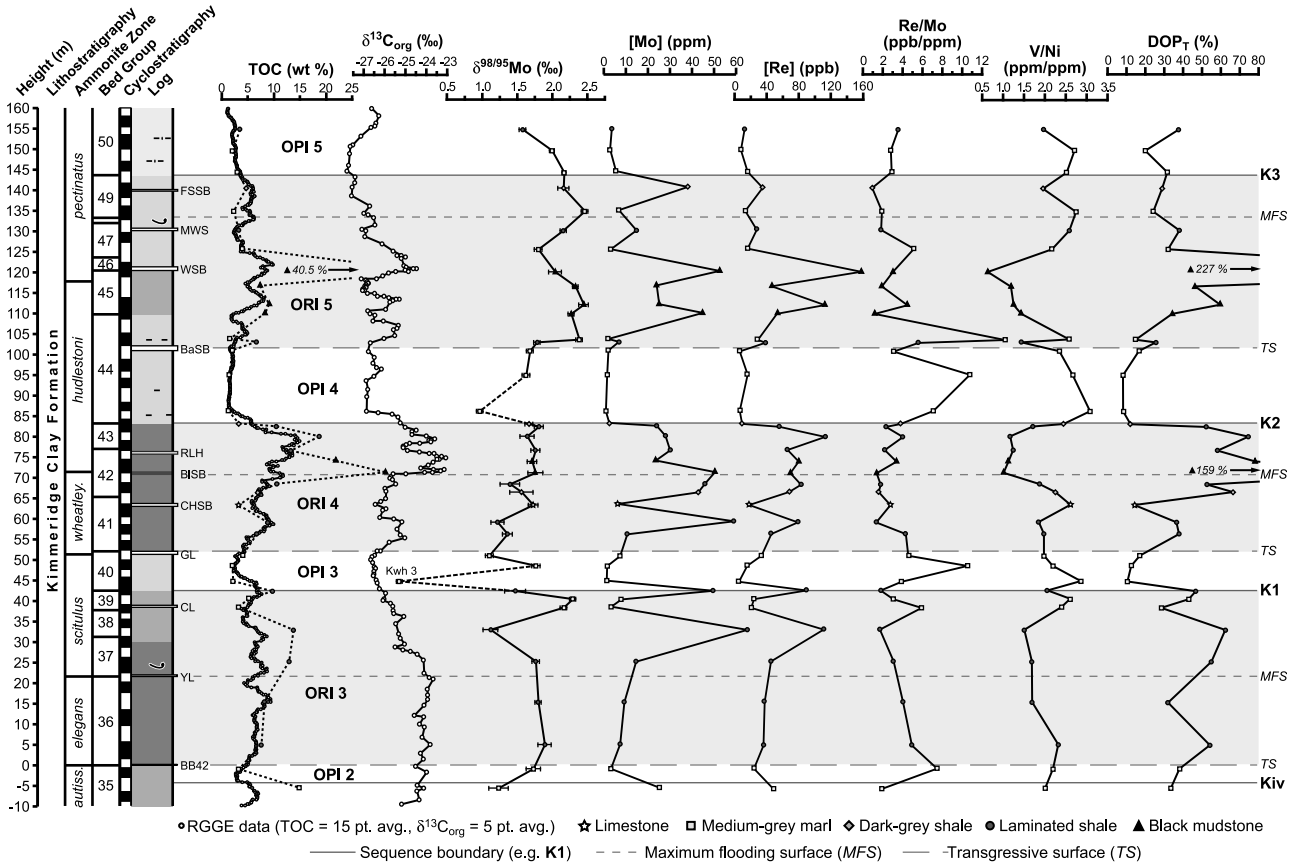

Figure 3. Variations in TOC, $\delta^{13}C_{org}$, $\delta^{98/95}Mo$, [Mo], [Re], Re/Mo, V/Ni, and DOP_T of samples from the KCF analyzed in this study plotted against stratigraphical position. The graphic log and biostratigraphical information are from the compilation of *Morgans-Bell et al.* [2001]. CHSB, Clavell's Hard Stone Band [*Coe*, 1992]. Other limestone horizon abbreviations are as in Figure 2. Cyclostratigraphy represents the long-term orbital obliquity cycles of ~38 ka, as defined by *Weedon et al.* [2004]. The high-resolution RGGE TOC and $\delta^{13}C_{org}$ data have been correlated with the coastal exposure log using the tie depths of separate marker horizons [*Morgans-Bell et al.*, 2001]. All other geochemical data are from this study. The sedimentary facies corresponding to the bed that the sample was taken from is reflected in the shape of each sample point. The positions of the sequence boundaries (Kiv, K1, K2, and K3), maximum flooding surfaces (MFS), and transgressive surfaces (TS) are from *Coe* [1992] and *Ahmadi and Coe* [1998]. The organic-rich intervals (ORIs) and intervening organic-poor intervals (OPIs) are labeled with the ORIs highlighted in gray.

lithologies [*Coe*, 1992; *Morgans-Bell et al.*, 2001] and include limestone (the Clavell's Hard Stone Band), medium dark to dark gray marl (henceforth medium gray marl), medium dark to dark gray to greenish-black shale (henceforth dark gray shale), dark gray to greenish-black to olive-black laminated shale (henceforth laminated shale), and grayish-black to brownish-black mudstone (henceforth black mudstone). The samples analyzed in this study have been correlated with the high-resolution $CaCO_3$, TOC, and $\delta^{13}C_{org}$ data obtained from the Rapid Global Geological Events (RGGE) project boreholes (Figures 2 and 3) using the tie depths of separate marker horizons described by *Morgans-Bell et al.* [2001].

[11] The $\delta^{98/95}Mo$ composition, major and minor element concentrations, and TOC, $CaCO_3$, and TS contents were determined for the selected samples at The Open University (Tables 1 and 2). The Mo isotope compositions and [Mo] and [Re] abundances were measured with a Nu Instruments MC-ICP-MS using the procedure described by *Pearce et al.* [2009]. The long-term $\delta^{98/95}Mo$ reproducibility of this protocol is 0.12‰, which is similar to that reported in other Mo isotope studies. Major and minor element concentrations were determined by X-ray fluorescence (XRF) analysis, using an ARL 8420+ dual goniometer wavelength dispersive XRF spectrometer, while TOC, $CaCO_3$, and TS contents were determined on ~200 mg samples using a LECO Instruments CNS-2000 elemental analyzer.

3. Results

3.1. $\delta^{98/95}Mo$ Variations

[12] Most $\delta^{98/95}Mo$ values determined in this study from the KCF are between 0.96‰ and 2.46‰, the only exception being sample Kwh 3, which has the lowest measured

Table 1. Stratigraphic and Geochemical Information for the Samples Analyzed in This Study[a]

Sample Name	Bed		Lithology	Ammonite Zone	Height (m)		$\delta^{98/95}$Mo (‰)	[Mo] (ppm)	[Re] (ppb)	Re/Mo (ppb/ppm)	TOC (wt %)	TS (wt %)	$CaCO_3$ (wt %)	DOP_T (%)
	Group	No.			Above Bed Base	Above Datum								
Kpe 34	50	12	L S	*Pe. pectinatus*	0.20	154.79	1.58 ± 0.05	3.54	12.55	3.54	3.45	1.79	1.77	37.58
Kpe 27	50	5	M-G M	*Pe. pectinatus*	1.30	149.63	2.00 ± 0.04	2.85	7.99	2.80	2.02	0.90	8.85	20.01
Kpe 23	50	1	M-G M	*Pe. pectinatus*	0.70	144.37	2.17 ± 0.03	5.54	16.04	2.89	2.98	1.34	15.28	31.60
Kpe 19	49	9	D-G S	*Pe. pectinatus*	0.32	140.50	2.16 ± 0.08	37.98	35.06	0.92	4.75	1.51	17.46	28.93
Kpe 13	49	2	M-G M	*Pe. pectinatus*	1.00	134.84	2.46 ± 0.05	6.94	13.29	1.91	2.31	1.18	16.38	24.23
Kpe 8	47	10	L S	*Pe. pectinatus*	0.32	130.21	2.16 ± 0.04	14.91	27.54	1.85	3.21	1.88	10.83	38.06
Kpe 4	47	1	M-G M	*Pe. pectinatus*	2.00	125.65	1.80 ± 0.06	3.22	16.51	5.13	4.03	1.23	24.84	32.07
Khu 40	45	25	B Mud	*Pe. hudlestoni*	0.10	120.12	2.04 ± 0.09	52.58	157.84	3.00	40.47	7.75	6.51	227.32
Khu 34	45	13	B Mud	*Pe. hudlestoni*	0.20	116.59	2.33 ± 0.04	23.91	46.16	1.93	7.38	2.06	40.55	46.43
Khu 28	45	6	B Mud	*Pe. hudlestoni*	0.86	112.19	2.45 ± 0.07	25.11	112.64	4.49	9.08	2.14	46.96	59.67
Khu 26	45	1	B Mud	*Pe. hudlestoni*	0.18	109.97	2.27 ± 0.04	44.86	53.01	1.18	8.33	1.03	42.32	34.20
Khu 22	44	5	M-G M	*Pe. hudlestoni*	0.60	103.68	2.38 ± 0.05	2.04	29.09	14.29	1.60	0.45	32.96	14.89
Khu 21	44	4	L S	*Pe. hudlestoni*	0.13	102.96	1.78 ± 0.05	6.86	38.30	5.58	6.67	0.72	36.05	25.53
Khu 19	44	1	M-G M	*Pe. hudlestoni*	17.62	100.85	1.68 ± 0.05	2.01	6.22	3.09	2.05	0.51	28.01	16.63
Khu 18	44	1	M-G M	*Pe. hudlestoni*	11.73	94.96	1.62 ± 0.05	1.50	16.09	10.75	1.47	0.34	25.64	8.14
Khu 16	44	1	M-G M	*Pe. hudlestoni*	3.00	86.23	0.96 ± 0.05	0.91	6.45	7.10	1.15	0.29	34.34	8.25
Khu 15	43	11	D-G S	*Pe. hudlestoni*	0.20	83.11	1.67 ± 0.06	2.41	9.13	3.78	3.23	0.44	21.62	12.15
Khu 14	43	9	L S	*Pe. hudlestoni*	0.65	82.46	1.81 ± 0.06	23.90	55.72	2.33	10.47	1.98	1.69	52.10
Khu 12	43	5	L S	*Pe. hudlestoni*	0.57	80.04	1.64 ± 0.10	28.05	113.13	4.03	18.73	2.24	9.07	74.61
Khu 10	42	25	L S	*Pe. hudlestoni*	0.32	76.70	1.76 ± 0.06	30.00	66.13	2.20	13.22	1.90	21.41	58.26
Khu 8	42	20	B Mud	*Pe. hudlestoni*	0.54	73.98	1.71 ± 0.07	23.68	79.87	3.37	21.79	3.22	4.83	78.12
Kwh 28	42	12	B Mud	*Pe. wheatleyensis*	0.38	71.21	1.76 ± 0.11	50.42	69.30	1.37	31.42	4.65	7.00	158.46
Kwh 22	42	7	L S	*Pe. wheatleyensis*	0.10	68.41	1.40 ± 0.14	45.93	82.94	1.81	10.58	2.15	6.03	52.70
Kwh 19	42	4	D-G S	*Pe. wheatleyensis*	0.10	66.55	1.56 ± 0.17	42.73	68.17	1.60	6.89	3.42	3.91	66.44
Kwh 15	41	22	Lst	*Pe. wheatleyensis*	0.35	63.39	1.73 ± 0.07	6.47	18.03	2.79	3.25	0.77	41.56	14.18
Kwh 12	41	15	L S	*Pe. wheatleyensis*	0.10	59.24	1.22 ± 0.09	58.98	79.09	1.34	8.79	1.25	33.54	36.45
Kwh 9	41	8	L S	*Pe. wheatleyensis*	0.15	56.31	1.36 ± 0.07	10.64	46.05	4.33	6.71	1.22	12.45	37.88
Kwh 5	40	3	M-G M	*Pe. wheatleyensis*	6.42	51.05	1.10 ± 0.06	7.38	33.53	4.54	3.97	0.43	38.09	17.13
Kwh 4	40	3	M-G M	*Pe. wheatleyensis*	3.92	48.55	1.77 ± 0.06	1.49	15.69	10.53	2.11	0.40	40.16	12.52
Kwh 3	40	3	M-G M	*Pe. wheatleyensis*	0.21	44.84	−0.19 ± 0.04	1.37	5.33	3.89	2.16	0.45	34.07	10.53
Ksc 17	39	9	L S	*Pe. scitulus*	0.47	42.49	1.47 ± 0.15	49.60	89.78	1.81	9.74	1.64	19.73	46.81
Ksc 15	39	6	M-G M	*Pe. scitulus*	0.87	40.46	2.29 ± 0.04	7.97	24.34	3.05	5.14	1.31	15.31	42.91
Ksc 14	39	2	M-G M	*Pe. scitulus*	0.26	38.43	2.16 ± 0.05	3.48	20.61	5.92	3.28	0.75	15.73	28.46
Ksc 10	38	6	L S	*Pe. scitulus*	0.40	32.97	1.12 ± 0.10	65.11	111.12	1.71	13.81	2.40	16.70	62.35
Ksc 4	37	11	L S	*Pe. scitulus*	0.10	25.32	1.76 ± 0.05	14.64	45.27	3.09	12.88	2.16	4.59	55.01
Kel 19	36	30	L S	*Pe. elegans*	0.34	15.33	1.80 ± 0.04	9.24	37.38	4.05	8.18	1.53	5.32	32.02
Kel 7	36	8	L S	*Pe. elegans*	0.34	4.98	1.89 ± 0.10	7.34	36.13	4.92	7.55	2.09	4.77	54.17
Kau 105	35	49	M-G M	*A. autissiodorensis*	1.60	−0.85	1.73 ± 0.10	3.21	23.98	7.46	3.20	1.12	2.71	38.08
Kau 101	35	39	M-G M	*A. autissiodorensis*	0.05	−5.60	1.23 ± 0.14	25.11	48.27	1.92	14.86	2.01	10.94	33.50

[a]The lithology of each sample reflects that defined for the corresponding bed number by *Morgans-Bell et al.* [2001]. Lst, limestone; M-G M, medium gray marl; D-G S, dark gray shale; L S, laminated shale; B Mud, black mudstone. $\delta^{98/95}$Mo, [Mo], and [Re] were measured with a Nu Instruments MC-ICP-MS at Open University, as described by *Pearce et al.* [2009]. Uncertainties for $\delta^{98/95}$Mo reflect the 2 standard error of each measurement; the long-term $\delta^{98/95}$Mo reproducibility is 0.12‰ (2 SD). TOC, TS, and $CaCO_3$ were obtained using a LECO Instruments CNS-2000 elemental analyzer.

$\delta^{98/95}$Mo value of −0.19‰ (Figure 3 and Table 1). There is no notable relationship between $\delta^{98/95}$Mo and facies type, although some stratigraphic trends can be discerned through the KCF: $\delta^{98/95}$Mo increases from 1.23‰ at the top of the *autissodorensis* zone to 2.29‰ by the middle of the *scitulus* zone and then decreases to ~1.7‰ in the upper *scitulus* zone, at the end of ORI 3 (ignoring the single exceptionally low value of −0.19‰ at the start of OPI 3). $\delta^{98/95}$Mo values remain fairly constant at ~1.7‰ through the upper *scitulus* and lower *wheatleyensis* zones (representing ORI 4), until the *hudlestoni* zone where they drop to 0.96‰. This second decrease coincides with the end of ORI 4. $\delta^{98/95}$Mo compositions increase to ~2.4‰ by the middle of the *hudlestoni* zone (the start of ORI 5) and remain at generally higher values than found during ORIs 3 and 4 (i.e., between 1.80‰ and 2.46‰) throughout the upper *hudlestoni* and lower *pectinatus* zones. There is a progressive decrease in $\delta^{98/95}$Mo from 2.46‰ to 1.58‰ toward the end of ORI 5 (between the middle *pectinatus* zone and upper *pectinatus* zone, the top of the analyzed section). These variations in $\delta^{98/95}$Mo are thus clearly associated with the long-term cycles in TOC, with lower $\delta^{98/95}$Mo values occurring during the OPIs and higher $\delta^{98/95}$Mo values during the ORIs (Figure 3).

3.2. Mo and Re Abundances and Re/Mo Ratios

[13] In contrast to $\delta^{98/95}$Mo, Mo and Re abundances vary considerably between the upper *autissodorensis* and upper *pectinatus* zones. Molybdenum concentrations range from 0.9 to 65.1 ppm, while [Re] varies between 5.3 and 157.8 ppb. High and low concentrations of both elements occur intermittently throughout the succession (Figure 3). Particularly abrupt fluctuations in [Mo] and [Re] are apparent in the *scitulus*, *wheatleyensis*, *hudlestoni*, and *pectinatus* zones and are associated with changes in facies; higher concentrations of both metals occur in the more organic-rich units (i.e., the black mudstones and laminated shales), while lower

Table 2. Major and Minor Element Abundance Information Determined Using an ARL 8420+ Dual Goniometer Wavelength Dispersive XRF Spectrometer

Sample Name	SiO_2 (wt %)	TiO_2 (wt %)	Al_2O_3 (wt %)	Fe_2O_3 (wt %)	MnO (wt %)	MgO (wt %)	Cr (ppm)	Cu (ppm)	Ni (ppm)	Sr (ppm)	Th (ppm)	U (ppm)	V (ppm)	Zr (ppm)	V/Ni (ppm/ppm)
Kpe 34	48.22	0.82	19.09	5.84	0.02	1.22	138.90	32.90	68.30	150.90	14.20	3.80	134.80	150.70	1.97
Kpe 27	43.78	0.71	16.01	5.50	0.02	1.28	125.40	19.70	48.50	153.70	11.40	2.10	131.30	140.50	2.71
Kpe 23	39.97	0.67	14.90	5.22	0.02	1.03	117.70	22.40	47.70	254.90	12.10	4.10	120.30	129.00	2.52
Kpe 19	41.79	0.66	16.69	6.41	0.02	1.49	105.00	23.10	64.40	198.70	11.10	10.30	126.00	118.50	1.96
Kpe 13	15.31	0.27	5.60	5.98	0.03	0.41	125.40	21.20	46.80	207.70	10.90	3.00	128.40	112.60	2.74
Kpe 8	43.46	0.67	18.42	6.09	0.02	1.31	125.80	26.50	59.90	189.60	11.20	4.90	154.80	105.60	2.58
Kpe 4	37.20	0.55	13.75	4.72	0.02	1.18	106.30	25.60	51.50	224.70	10.80	3.80	111.70	98.60	2.17
Khu 40	37.58	0.62	12.93	4.19	0.01	0.85	40.10	60.70	88.70	109.90	4.10	6.20	56.30	51.30	0.63
Khu 34	20.07	0.28	7.75	5.44	0.03	0.76	51.60	37.60	72.40	256.90	3.40	5.90	86.00	49.50	1.19
Khu 28	16.98	0.23	6.39	4.40	0.02	0.61	46.50	42.20	61.60	251.70	3.30	4.90	77.10	42.30	1.25
Khu 26	22.47	0.29	8.16	3.69	0.02	0.84	53.00	40.40	65.90	248.50	5.10	5.10	94.30	51.90	1.43
Khu 22	36.03	0.57	13.86	3.72	0.02	1.78	94.10	19.40	42.10	317.90	9.90	3.30	108.60	95.50	2.58
Khu 21	30.46	0.40	10.93	3.49	0.02	1.06	76.60	39.40	61.60	264.40	7.10	2.50	88.70	68.20	1.44
Khu 19	38.44	0.61	14.36	3.74	0.02	1.59	101.90	22.50	46.80	309.80	11.80	3.00	109.80	102.60	2.35
Khu 18	41.15	0.66	14.70	5.17	0.02	1.91	104.70	17.70	44.50	294.10	11.20	2.40	118.70	119.20	2.67
Khu 16	38.71	0.59	12.42	4.28	0.02	1.95	91.90	17.20	34.30	383.90	8.20	3.30	105.60	120.40	3.08
Khu 15	41.80	0.68	15.58	4.48	0.02	1.69	115.90	21.70	48.40	276.30	11.90	2.50	118.20	123.70	2.44
Khu 14	49.06	0.76	17.11	4.66	0.01	1.06	115.10	42.10	72.70	90.60	13.20	3.90	124.30	136.80	1.71
Khu 12	37.39	0.59	13.21	3.69	0.01	0.82	89.90	40.60	90.60	135.10	9.40	5.40	106.00	110.30	1.17
Khu 10	34.00	0.53	11.47	4.02	0.01	0.73	86.20	34.50	74.70	136.40	9.80	3.70	92.50	103.60	1.24
Khu 8	52.54	0.88	19.84	5.08	0.02	1.25	79.50	31.60	77.70	115.40	10.00	5.50	87.70	123.20	1.13
Kwh 28	26.72	0.46	9.45	3.61	0.01	0.69	48.90	34.60	67.00	111.50	6.30	3.30	67.80	88.70	1.01
Kwh 22	43.94	0.74	16.04	5.01	0.02	1.11	114.40	46.00	78.20	174.90	11.50	5.20	146.50	136.90	1.87
Kwh 19	44.44	0.70	17.50	6.32	0.02	1.11	111.80	51.40	72.70	150.40	10.20	4.20	163.40	126.70	2.25
Kwh 15	34.30	0.50	8.43	6.66	0.04	4.30	72.90	23.60	30.80	199.60	6.00	2.50	80.40	132.30	2.61
Kwh 12	28.49	0.46	10.63	4.20	0.02	0.70	75.10	41.30	78.00	227.90	8.90	7.10	144.50	90.80	1.85
Kwh 9	47.19	0.71	14.43	3.97	0.01	0.94	105.60	40.10	60.10	174.20	10.40	4.70	118.80	155.60	1.98
Kwh 5	31.90	0.46	11.67	3.11	0.02	1.52	76.10	29.00	53.00	376.70	6.70	3.40	104.70	81.70	1.98
Kwh 4	32.94	0.51	11.45	3.97	0.02	2.45	80.90	20.30	41.90	375.90	9.90	2.60	91.60	99.10	2.19
Kwh 3	36.65	0.56	12.33	5.26	0.03	2.22	89.00	17.60	36.70	364.70	10.30	0.20	104.90	116.80	2.86
Ksc 17	35.47	0.61	14.24	4.32	0.01	0.88	90.70	41.90	86.10	212.90	9.30	8.10	177.70	114.20	2.06
Ksc 15	48.87	0.72	12.84	3.76	0.01	0.96	92.10	28.60	47.80	214.90	10.40	3.30	124.60	167.10	2.61
Ksc 14	54.45	0.75	11.47	3.24	0.02	0.99	79.00	21.50	32.40	170.80	10.10	3.50	77.50	210.50	2.39
Ksc 10	32.53	0.55	12.51	4.74	0.01	0.73	88.90	53.50	89.30	174.40	9.10	5.00	134.50	108.40	1.51
Ksc 4	45.42	0.74	16.16	4.83	0.02	0.96	103.60	40.20	73.30	112.40	11.30	4.30	123.70	144.10	1.69
Kel 19	48.13	0.76	17.47	5.88	0.03	0.99	114.50	34.20	83.50	114.90	13.10	2.20	141.60	140.20	1.70
Kel 7	51.19	0.87	18.38	4.73	0.02	0.89	124.20	30.60	57.10	185.20	10.80	3.80	132.40	169.40	2.32
Kau 105	63.45	0.86	14.87	3.63	0.01	0.81	95.20	19.00	46.60	103.80	9.20	3.80	102.30	282.00	2.20
Kau 101	38.18	0.64	13.64	7.38	0.03	1.52	102.40	27.70	60.40	132.50	9.70	5.30	121.30	137.60	2.01

concentrations occur in the less organic-rich lithologies (i.e., the medium gray shale and the limestone). The apparent absence of progressive changes in [Mo] and [Re] in the analyzed section is likely to reflect the relatively low sample resolution across the sharp lithological contacts. Nevertheless, both [Mo] and [Re] (and consequently Re/Mo ratios) correlate well with the long-term TOC cycles, with higher concentrations of both metals found in the three ORIs; the average [Mo] and [Re] of the ORIs are 25.80 ppm and 58.24 ppb, respectively, while the average [Mo] and [Re] of the OPIs are 4.78 ppm and 16.77 ppb, respectively (Figure 3). Similarly, Re/Mo ratios are lower during the ORIs (averaging 3.33) and are higher during the OPIs (averaging 5.19).

3.3. TOC, V/Ni, and DOP_T

[14] The TOC contents of samples analyzed in this study closely match those of the RGGE core record, although the TOC concentrations in the RGGE data set (Figure 3) are lower as they are derived from ~1 mg aliquots of larger samples collected over 20 cm intervals and have been further smoothed by taking a 15-point moving average. By definition, the three ORIs have the highest TOC contents (varying between ~5 and 40.5 wt %), while the intervening OPIs have lower TOC values that are typically <5 wt %. The highest measured TOC contents of 31.4 and 40.5 wt % occur in the Blackstone Band and just below the White Stone Band (Bed Group 40; Bed 25), respectively. V/Ni ratios (Table 2) and DOP_T have an antiphase relationship that varies stratigraphically in a manner similar to that of TOC (Figure 3). Lower V/Ni ratios (<2.5) and higher DOP_T values (>25%) are recorded from the three ORIs, while higher V/Ni ratios (>2.5) and lower DOP_T values (<20%) are associated with the OPIs. The extremely TOC-rich Blackstone Band and Bed 40/25 are also associated with the lowest V/Ni ratios (0.63 and 1.01) and the highest DOP_T values (159% and 227%), respectively.

4. Discussion

4.1. Depositional Environment of the KCF in Dorset

[15] The paleoredox proxies used in this study all indicate that none of the samples were deposited in an oxic environment. DOP_T is never less than ~10%, and TOC does not

decrease below 1.15 wt % (Figure 3). The lowest observed $\delta^{98/95}$Mo value of −0.19‰ (sample Kwh 3; Figure 3) is similar to the mean continental $\delta^{98/95}$Mo value of ~0‰ [*Siebert et al.*, 2003], suggesting that the Mo in this sample is dominated by the detrital component. This interpretation is supported by the fact that the Mo concentration of this sample is only 1.4 ppm and that it plots significantly below the expected $\delta^{98/95}$Mo versus 1/[Mo] trendline. The observation that all other $\delta^{98/95}$Mo values are above 0.96‰ implies that the depositional environment throughout the studied interval was oxygen deficient and predominantly anoxic or euxinic, in agreement with previous findings [e.g., *Piper and Calvert*, 2009; *Tribovillard et al.*, 2004b].

[16] The inference from the $\delta^{98/95}$Mo data that the limestone, medium gray marl, and dark gray shale facies in the KCF were deposited under mildly reducing conditions is supported by the DOP_T/TOC and TS/TOC relationships (Figure 4). These relatively organic-poor samples (TOC values of 1–7 wt %) define positive linear relationships that intercept close to the origin for both DOP_T/TOC and TS/TOC, suggesting that that there is little or no syngenetic pyrite present within these samples (i.e., euxinic conditions did not extend above the sediment-water interface at those times). In particular, the gradient defined by the TS/TOC values for these samples (0.41; Figure 4b) is the same as that suggested by *Raiswell and Berner* [1985] for oxic to suboxic sedimentary deposits. The relatively organic-rich samples (TOC contents typically >7 wt %) from the laminated shale and black mudstone facies define DOP_T/TOC and TS/TOC relationships that have shallower slopes and positive intercepts on the *y* axis (Figure 4). This observation implies that these facies correspond to more strongly reducing (anoxic to euxinic) conditions in which syngenetic pyrite was able to form in the water column due to the (perhaps intermittent) presence of free H_2S. The presence of sulfidized organic matter and sygnetic pyrite crystals in the TOC-rich Kimeridgian sedimentary deposits of Yorkshire [*Tribovillard et al.*, 2004a] supports this inference.

[17] Trace metal paleoredox data also suggest that the intensity of reducing conditions varied locally during the deposition of the KCF. Changes in the Re/Mo and V/Ni ratios are inversely correlated with DOP_T fluctuations (Figure 3). These proxies imply that the organic-rich intervals were deposited under more strongly reducing conditions than the organic-poor intervals. Similar variations are seen in the relative enrichments of Mo and U (Figure 4d). Lower Mo/U ratios are recorded in the less organic-rich sedimentary deposits (averaging 4.9 in the medium gray shales), while the most organic-rich sedimentary deposits have higher Mo/U ratios, with an average of 23.8 in the black mudstone facies. Mo/U ratios below that of present-day seawater (~7.5–7.9) [*Algeo and Tribovillard*, 2009] indicate that deposition occurred under suboxic conditions, while Mo/U ratios above seawater suggest enhanced Mo accumulation under sulfidic conditions. The Mo/U relationship defined by samples from the KCF (Figure 4d) is similar to that observed in sedimentary deposits from the Cariaco Basin, for which a particulate shuttle has been suggested as a means of achieving the high-Mo enrichments [*Algeo and Tribovillard*, 2009]. This process, which is linked to Mn-Fe redox cycling, is aided by variations in water column redox and supports other evidence showing that the depositional environment of the KCF varied over time [e.g., *Wignall and Meyers*, 1988; *Wignall and Newton*, 2001]. Local redox conditions during the accumulation of the KCF in Dorset are consequently inferred to have varied from suboxic to euxinic and can be directly related to the TOC content and to sedimentary facies.

4.2. Extent of Marine Anoxia During the Kimmeridgian

4.2.1. $\delta^{98/95}$Mo, Astronomical Cycles, and Relative Sea Level Change

[18] Relatively little variation is observed in $\delta^{98/95}$Mo within any one ORI or OPI of the KCF, despite a range of facies types being analyzed (Figure 3). This finding suggests that, within the sampling resolution of this study, $\delta^{98/95}$Mo was not significantly affected by the short-term changes in local facies type. Longer-term differences can be seen, however, between the mean $\delta^{98/95}$Mo compositions of the ORIs. The average $\delta^{98/95}$Mo value of sediments deposited in ORI 5 (2.18‰) is close to that of seawater and is therefore similar to the Mo isotope composition of sediments deposited in modern day euxinic environments (e.g., the Black Sea) [*Neubert et al.*, 2008], whereas the average $\delta^{98/95}$Mo values of sedimentary deposits from ORIs 3 and 4 (1.79‰ and 1.60‰, respectively) are closer to those observed in anoxic environments (~1.7‰) [*Poulson et al.*, 2006; *Siebert et al.*, 2006]. Since the DOP_T/TOC and TS/TOC crossplots indicate that the organic-rich facies were deposited under strongly reducing/euxinic conditions (Figure 4) and biomarker evidence from the presence of isorenieratane suggests that photic zone euxinia occurred at various intervals throughout the KCF [*Sinninghe Damsté et al.*, 2001], there is no reason to suspect that the lower mean $\delta^{98/95}$Mo values of ORIs 3 and 4 reflect deposition under less reducing conditions. Differences in the $\delta^{98/95}$Mo values of the three ORIs covered in this study are therefore thought to reflect changes in the $\delta^{98/95}$Mo composition of global seawater caused by variations in the areal extent of reducing depositional conditions.

[19] The $\delta^{98/95}$Mo value of seawater depends on the global proportion of oxic to euxinic/highly reducing sedimentation [*Anbar*, 2004; *Arnold et al.*, 2004; *Ling et al.*, 2005], such that an increase in the areal extent of reducing sedimentation would decrease $\delta^{98/95}Mo_{seawater}$ and lower $\delta^{98/95}$Mo in the coeval euxinic sediments. On the basis of a two end-member model for Mo removal from the oceans (i.e., considering oxic and euxinic sinks only) [*Ling et al.*, 2005], the mean seawater $\delta^{98/95}$Mo values of 1.79‰ and 1.60‰ during ORIs 3 and 4 suggest a twofold or threefold increase in the proportion of Mo burial in euxinic sediments (with respect to the present-day oceans), respectively. In reality, however, some of the decrease in $\delta^{98/95}$Mo during these two ORIs will have been caused by an increase in the proportion of Mo burial in suboxic to anoxic (i.e., noneuxinic) reducing sediments on continental margins [cf. *McManus et al.*, 2006; *Siebert et al.*, 2006].

[20] A close relationship between the timing of the ORIs and third-order relative sea level fluctuations in the

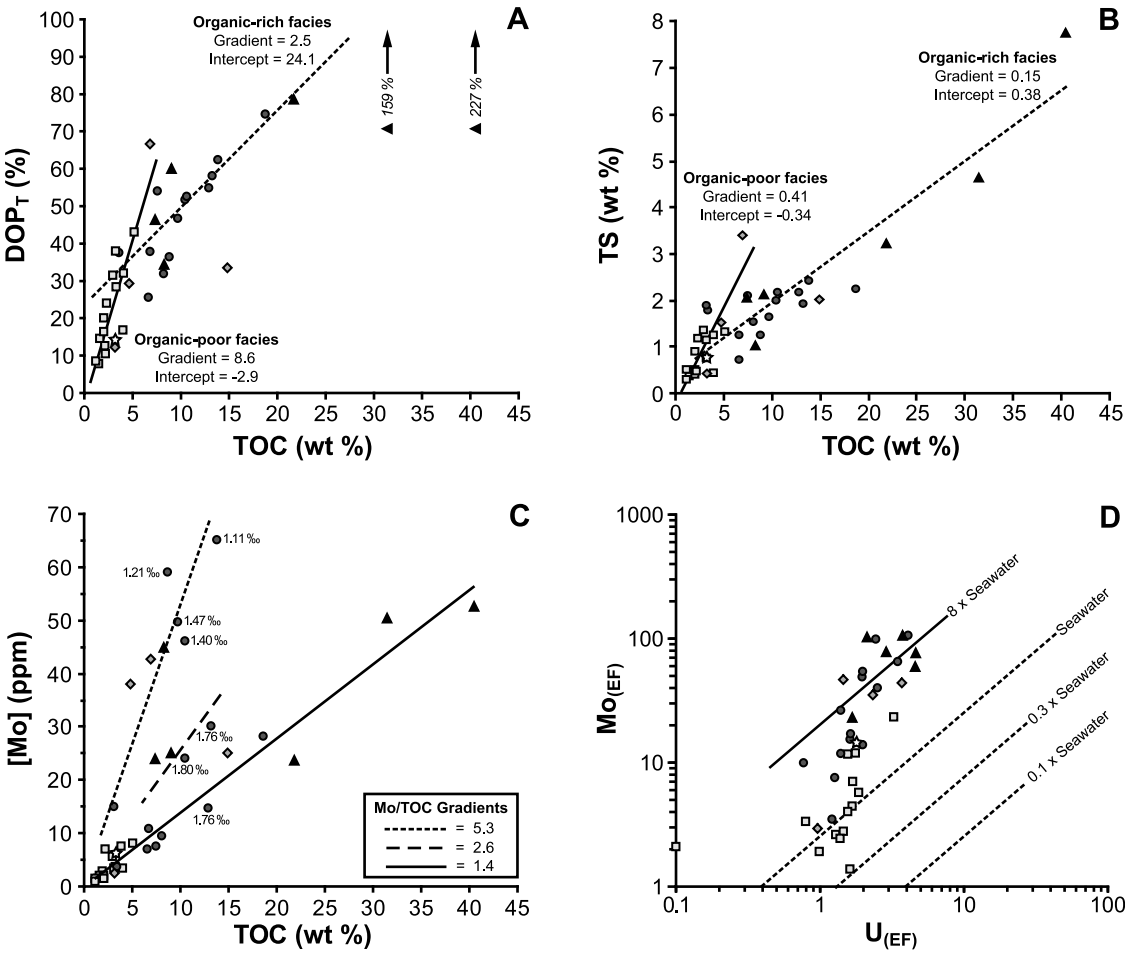

Figure 4. Relationships between (a) DOP_T and TOC, (b) TS and TOC, (c) [Mo] and TOC, and (d) $Mo_{(EF)}$ and $U_{(EF)}$ for the KCF. The shape of each sample point reflects its lithology (see Figure 3 for key). Different relationships are defined by the organic-poor facies (TOC 1–7 wt %; medium gray marl and dark gray shale) and the organic-rich facies (TOC >7 wt %; laminated shale and black mudstone) in the DOP_T versus TOC and TS versus TOC crossplots (Figures 4a and 4b, respectively). In both instances, the organic-rich sedimentary deposits have positive intercepts that indicate sygenetic pyrite formation under strongly reducing (anoxic to euxinic) conditions. Intercepts for the organic-poor sedimentary deposits are zero to negative, implying that these deposits contain only diagenetic pyrite formed under less reducing (suboxic to anoxic) conditions. [Mo]/TOC gradients recorded in the KCF (Figure 4c) are lower than for present-day anoxic basins [*Algeo and Lyons*, 2006] but are not thought to reflect basinal restriction during the Kimmeridgian, as the organic-rich facies have Mo/U ratios that are up to 8 times higher than that of seawater (Figure 4d). In addition, Mo/U ratios of the KCF organic-rich facies do not decrease below seawater (e.g., to 0.3 times or 0.1 times the present-day levels indicated by the dashed lines), indicating that the KCF was deposited in a sulfidic and non-Mo-limited environment [see *Algeo and Tribovillard*, 2009, for more detail]. This inference is supported by the observation that $\delta^{98/95}$Mo decreases as [Mo] increases in the laminated shale facies (Figure 4c), which is the inverse relationship to that expected during basinal restriction. In conjunction these trace metal proxies show that the redox conditions varied from suboxic to euxinic during the accumulation of the KCF and that the basin never became strongly restricted for a significant period of time, if at all.

Kimmeridgian [*Coe*, 1992; *Tribovillard et al.*, 2004b] supports the hypothesis that flooding of the continental margins through the Laurasian Seaway may have aided the generation of widespread stagnant and reducing depositional conditions during the ORIs. Sequence stratigraphic frameworks for the KCF in Dorset indicate that the sequence boundaries (representing periods of relative sea level fall at the end of a marine highstand) occur near the top of bed group 35 and at the base of bed groups 40, 44, and 50 [*Ahmadi*, 1997; *Ahmadi and Coe*, 1998; *Coe*, 1992; *Taylor et al.*, 2001]. Three of these surfaces (K1, K2, and K3) correspond closely with the end of ORIs 3, 4, and 5, respectively (Figure 3). Similarly, the transgressive surfaces that define the onset of relative sea level rise occur near the start of the

three ORIs (at the base of bed groups 36 and 41 and near the middle of bed group 44), while the highest TOC levels within each ORI broadly correspond to the inferred maximum flooding surfaces (Figure 3). These observations suggest that periods of high relative sea level aided the deposition of organic-rich mudrocks and hence the formation of the ORIs. Conversely, periods of low relative sea level resulted in the redeposition of sediments from the margins into the basin, while water depth was insufficient to allow widespread reducing conditions to develop across the Laurasian Seaway [*Coe*, 1992; *Piper and Calvert*, 2009; *Tribovillard et al.*, 2004b].

4.2.2. Assessment of Basinal Restriction

[21] In theory, it is possible that changes in sedimentary $\delta^{98/95}$Mo values reflect variations in the degree of restriction of the depositional basin, as the $\delta^{98/95}$Mo composition of dissolved Mo will decrease relative to that of coeval seawater if the reservoir becomes dominated by isotopically light riverine Mo ($\delta^{98/95}Mo_{riverine}$ = ~0.8‰ [*Archer and Vance*, 2008]). Such effects will also be associated with a significant decrease in the abundance of Mo within the basin, as the concentration of Mo in the dissolved riverine load is significantly lower than that of seawater. Variations in [Mo]/TOC ratios have consequently been proposed as a proxy for the degree of restriction of a marine basin, and reducing basins have been shown to display different [Mo]/TOC relationships according to the extent of Mo drawdown [*Algeo and Lyons*, 2006; *McArthur et al.*, 2008]. Restricted basins such as the Black Sea have low [Mo]/TOC gradients of ~4.5, while partially restricted basins such as the Cariaco Basin have higher [Mo]/TOC gradients of ~25 [*Algeo and Lyons*, 2006]. The samples analyzed from the KCF in this study typically have [Mo]/TOC gradients below those of the present-day reducing basins, with values ranging from 1.4 to 5.3 (Figure 4c). Other things being equal, this observation could be consistent with a partial to strong degree of basinal restriction for the KCF. However, there is no evidence for limited Mo renewal in the $Mo_{(EF)}/U_{(EF)}$ relationship (Figure 4d), as unlike samples from the Black Sea [*Algeo and Tribovillard*, 2009], the Mo/U ratios of organic-rich samples from the KCF do not fall below the composition of seawater. This finding suggests that basin reservoir effects are not responsible for the low [Mo]/TOC gradients within the KCF and that instead the relationship is more likely to be controlled by the very high organic carbon content of the KCF deposits.

[22] The interpretation that the Wessex Basin was not restricted during the Kimmeridgian is also supported by lithological and sequence stratigraphical evidence that implies that the ORIs were deposited during marine highstands [e.g., *Tribovillard et al.*, 2004b]. In addition, the fact that samples from the organic-rich laminated shale facies display a clear decrease in $\delta^{98/95}$Mo as [Mo] increases (Figure 4c) is inconsistent with enhanced scavenging of isotopically light riverine Mo from a hypothetically restricted basin, as the abundance of Mo would be expected to decrease under such conditions. There is also no evidence for significant riverine discharge into the Laurasian Seaway during the Kimmeridgian, as the region was dominated by low-lying landmasses and the climate is thought to have been relatively arid [*Abbink et al.*, 2001; *Wignall and Ruffell*, 1990]. Finally, if basinal restriction was the cause for the lower $\delta^{98/95}$Mo values in ORIs 3 and 4, then ORI 5 should display a similar if not more extreme trend (i.e., to even lower $\delta^{98/95}$Mo) owing to the fact that it was deposited after the period of highest relative sea level in the Kimmeridgian [*Coe*, 1992; *Taylor et al.*, 2001; *Tribovillard et al.*, 2004b], whereas the reverse trend is in fact observed. Taken together, these observations suggest that the long-term changes in the $\delta^{98/95}$Mo record of the KCF in Dorset reflect variations in the Mo composition of global seawater.

4.3. Comparison Between the KCF and the Toarcian OAE

[23] Several comparisons [e.g., *Sælen et al.*, 2000] have been made between the KCF and the Whitby Mudstone Formation (WMF) that was deposited in Yorkshire, United Kingdom, during the Toarcian (Early Jurassic). Part of the WMF accumulated during the Toarcian oceanic anoxic event (OAE), during which numerous organic-rich successions were deposited simultaneously worldwide [e.g., *Al-Suwaidi et al.*, 2010; *Cohen et al.*, 2007; *Jenkyns*, 1985, 1988, 2003; *Jenkyns et al.*, 2002]. The enhanced deposition of organic-rich sediment during the Toarcian was associated with a major perturbation to the global carbon cycle, characterized by a large negative carbon-isotope excursion that affected both the terrestrial and marine carbon reservoirs [*Hesselbo et al.*, 2000, 2007; *Kemp et al.*, 2005; *Schouten et al.*, 2000]. Variations in $\delta^{98/95}$Mo and other trace metal proxies in the WMF confirm that the global extent of anoxic sedimentation expanded appreciably during the OAE [*Archer and Vance*, 2008; *Pearce et al.*, 2008]. Furthermore, redox conditions during the OAE were found to fluctuate at the same time as astronomically paced variations in δ^{13}C [*Kemp et al.*, 2005], indicating that marine redox conditions at that time were closely related to climate [*Pearce et al.*, 2008]. On the basis of these observations, the deposition of TOC-rich successions during the Toarcian OAE can be attributed to the widespread expansion of marine anoxia that was most likely related to severely perturbed environmental conditions following the eruption of the Karoo-Ferrar LIP near the Pliensbachian-Toarcian boundary [*Cohen et al.*, 2004, 2007; *Hesselbo et al.*, 2000; *Pálfy and Smith*, 2000; *Pearce et al.*, 2008].

[24] Progressive changes in the areal extent of reducing deposition during the Toarcian OAE are illustrated by trends in the relationship between $\delta^{98/95}$Mo and 1/[Mo] (Figure 5a). The onset of reducing depositional conditions is defined by an increase in $\delta^{98/95}$Mo to 1.6‰ and a progressive increase in [Mo] that results in a well-defined oxic-anoxic linear relationship during the *Dactylioceras tenuicostatum* ammonite zone (Interval 1). The OAE itself (predominantly the *cleviceras exaratum* ammonite subzone; Interval 2) is characterized by a deviation away from this relationship, with $\delta^{98/95}$Mo decreasing as [Mo] increases. Because the local depositional environment remained euxinic [*Raiswell and Berner*, 1985] under conditions of rising sea level throughout the OAE, the decreases inferred for $\delta^{98/95}Mo_{seawater}$ at that time must have been caused by an expansion in the areal extent of marine anoxia [*Pearce et al.*, 2008]. This interval is also associated with a very low [Mo] (<10 ppm) for such

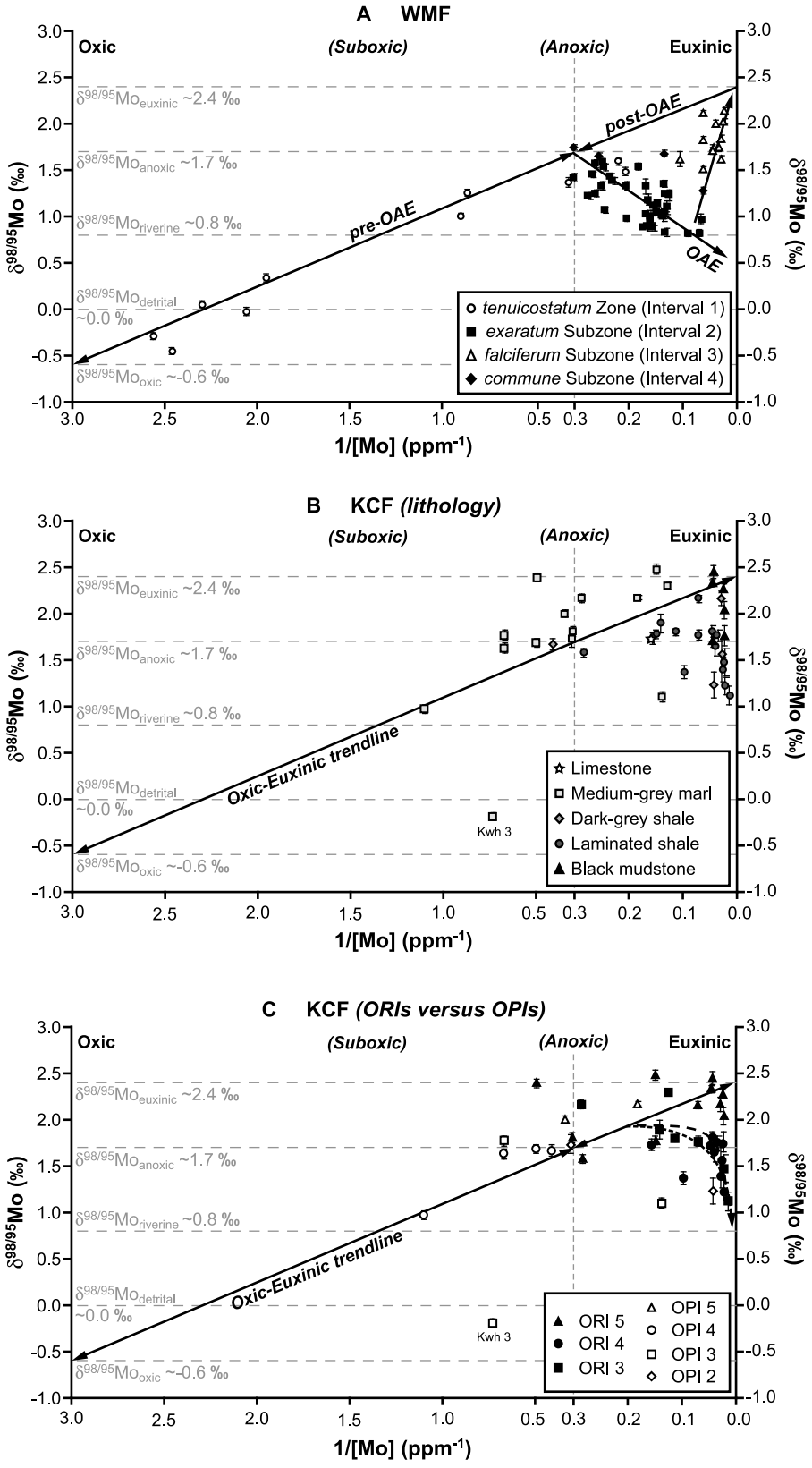
A WMF
Oxic
(Suboxic)
(Anoxic)
Euxinic
δ98/95Moeuxinic ~2.4 ‰
δ98/95Moanoxic ~1.7 ‰
δ98/95Moriverine ~0.8 ‰
δ98/95Modetrital ~0.0 ‰
δ98/95Mooxic ~-0.6 ‰
post-OAE
pre-OAE
OAE
tenuicostatum Zone (Interval 1)
exaratum Subzone (Interval 2)
falciferum Subzone (Interval 3)
commune Subzone (Interval 4)
δ98/95Mo (‰)
δ98/95Mo (‰)
1/[Mo] (ppm-1)
B KCF (lithology)
Oxic-Euxinic trendline
Kwh 3
Limestone
Medium-grey marl
Dark-grey shale
Laminated shale
Black mudstone
C KCF (ORIs versus OPIs)
ORI 5
ORI 4
ORI 3
OPI 5
OPI 4
OPI 3
OPI 2

Figure 5

organic-rich sedimentary deposits, which is an expected consequence of globally enhanced drawdown of the marine Mo inventory during the OAE [e.g., *Algeo*, 2004]. The end of widespread anoxia in the Toarcian is defined by an increase in $\delta^{98/95}$Mo and [Mo] during the *falciferum* and *commune* subzones (Intervals 3 and 4; Figure 5a), which reflect an increase in oxic Mo burial and the replenishment of the global oceanic Mo reservoir, respectively.

[25] In comparing the relationships between $\delta^{98/95}$Mo and 1/[Mo] in the WMF and the KCF, it should be remembered that the KCF section investigated in this study spans a much longer time interval than the WMF and also that samples from several different mudrock facies from the KCF have been analyzed. Samples from the medium gray marl in the KCF suggest a suboxic-euxinic relationship similar to that observed in the WMF (Figure 5b), although this relationship is not as well defined in the KCF as none of the samples analyzed represent fully oxic conditions. The $\delta^{98/95}$Mo values of the more organic-rich sedimentary deposits in the KCF generally fall below this oxic-euxinic trend and display a large variation in $\delta^{98/95}$Mo (between 1.12‰ and 2.45‰) at high [Mo]. Most of the variation in $\delta^{98/95}$Mo comes from sediments deposited during the three ORIs; comparison between the $\delta^{98/95}$Mo versus 1/[Mo] relationships for the ORIs and OPIs (Figure 5c) demonstrates that during each ORI $\delta^{98/95}$Mo decreased while [Mo] increased. The decrease in $\delta^{98/95}$Mo is particularly apparent in ORIs 3 and 4 and supports the suggestion that these periods were associated with a global expansion in the areal extent of reducing deposition. However, sedimentary deposits from the KCF are not associated with particularly low [Mo] (i.e., high 1/[Mo]), suggesting that the reduction in the marine Mo inventory during the ORIs was not as substantial as it was during the Toarcian OAE. This observation, in conjunction with the fact that $\delta^{98/95}$Mo decreases to only 1.12‰ (unlike 0.8‰ in the WMF), implies that the extent of highly reducing conditions during the deposition of the KCF was not as extensive as during the Toarcian OAE. Indeed, the decrease in $\delta^{98/95}$Mo during the ORIs may to some extent reflect the replacement of oxic sites of deposition with those where suboxic conditions prevailed, which would have diminished the dominant sink of isotopically light Mo in the oceans without significantly affecting the total amount of Mo in the oceans. The clear relationship between $\delta^{98/95}$Mo and 1/[Mo] for the KCF (Figure 5c) suggests that changes in marine redox occurred on a global scale during the Kimmeridgian and that these changes were directly related to the formation of the ORIs.

5. Conclusions

[26] This study provides the first Mo isotope data for the Kimmeridge Clay Formation (KCF), from its type section in Dorset, United Kingdom. Measured $\delta^{98/95}$Mo values, in conjunction with other trace metal paleoredox proxies (Mo and Re abundances, Re/Mo, Mo/U, Vi/Ni ratios and DOP_T) indicate that local depositional conditions of the KCF in Dorset between the *autissodorensis* and *pectinatus* zones were never fully oxic but varied from mildly reducing (suboxic) to strongly reducing (euxinic) and that changes in redox occurred on both short and long time scales. Interbed variations in trace metal abundances are directly linked to the TOC content and facies type of the sample, suggesting that the short-term changes in redox were governed by orbitally controlled climate changes that occurred cyclically during the accumulation of the KCF. Long-term variations in trace metal abundances and $\delta^{98/95}$Mo are associated with the formation of organic-rich intervals (ORIs) in the KCF that can be related to third-order (~700 ka) fluctuations in relative sea level.

[27] Differences in the mean $\delta^{98/95}$Mo value of the three ORIs examined in this study are best interpreted as reflecting changes in the $\delta^{98/95}$Mo composition of seawater caused by variations in the global extent of reducing depositional conditions. Flooding of continental margins during periods of marine highstand associated with the ORIs are interpreted to have promoted the expansion of reducing conditions. This hypothesis is supported by sequence stratigraphic frameworks for the KCF in Dorset, which indicate that transgressive surfaces occur near the start of the three ORIs while the sequence boundaries correspond closely with the end of ORIs. Conditions during the deposition of the intervening organic-poor intervals (OPIs) were less reducing, the OPIs having a higher detrital content as a consequence of relative sea levels being lower.

[28] Comparison between Mo isotope data from the KCF and the Toarcian Whitby Mudstone Formation (WMF) demonstrates that variations in $\delta^{98/95}$Mo and 1/[Mo] can be used in conjunction with other data to define the redox state(s) of palaeodepositional environments, as well as to

Figure 5. Comparison of the $\delta^{98/95}$Mo and 1/[Mo] relationships in (a) the Whitby Mudstone Formation (WMF) and (b and c) the Kimmeridge Clay Formation (KCF). Note that the 1/[Mo] scale is expanded below 0.3 ppm^{-1} and that the position of the "anoxic-euxinic" boundary at 0.3 ppm^{-1} is arbitrary. The $\delta^{98/95}$Mo compositions of the oceanic sources (detrital and riverine from *Siebert et al.* [2003] and *Archer and Vance* [2008], respectively) and sinks (oxic, anoxic and euxinic from *Poulson et al.* [2006]) are shown for reference. All data for the WMF are from *Pearce et al.* [2008]: Intervals 1–4 in the WMF reflect periods of deposition before, during, and after the Toarcian OAE. Decreases in $\delta^{98/95}$Mo combined with relatively low [Mo] during Interval 2 reflect the widespread expansion of anoxic deposition during the Toarcian OAE [*Pearce et al.*, 2008]. Data for the KCF are from this study and are shown according to lithology (Figure 5b) and whether they occur during an organic-poor interval (OPI) or organic-rich interval (ORI) (Figure 5c). Samples from the medium gray marl facies are generally close to the inferred oxic-euxinic trendline, with the exception of sample Kwh 3 that falls below this trend due to the predominance of the detrital Mo contribution. No notable trends are observed in other facies types, although samples deposited during ORIs 3 and 4 display decreases in $\delta^{98/95}$Mo and increases in [Mo], as highlighted by the dashed lines (short dash, ORI 3; long dash, ORI 4). These trends in ORIs 3 and 4 are consistent with an expansion in the areal extent of reducing sedimentation during these intervals of high relative sea level.

estimate the areal extent of reducing sedimentation globally. Our observations also suggest that the Mo isotope system in Jurassic seawater responded to changes in redox conditions in a manner that is consistent with its behavior in present-day sedimentary environments. Similar patterns of change in $\delta^{98/95}$Mo can therefore be anticipated for other episodes during which enhanced accumulation of marine organic matter occurred.

[29] **Acknowledgments.** We gratefully acknowledge John Watson for his assistance with the LECO and XRF analyses. We thank Kevin Burton, David Kemp, and colleagues at Open University for the useful discussions and guidance; Hugh Jenkyns and Nicolas Tribovillard for constructive comments on an earlier draft of the manuscript; and Christopher Charles for editorial advice. C. R. Pearce was supported by a NERC Ph.D. studentship (NER/S/A/2003/11301).

References

Abbink, O., J. Targarona, H. Brinkhuis, and H. Visscher (2001), Late Jurassic to earliest Cretaceous palaeoclimatic evolution of the southern North Sea, *Global Planet Change*, *30*, 231–256, doi:10.1016/S0921-8181(01)00101-1.

Ahmadi, Z. M. (1997), Sequence stratigraphy using wireline logs from the Upper Jurassic of England, Ph.D. thesis, Univ. of Durham, Durham, N. C.

Ahmadi, Z. M., and A. L. Coe (1998), Methods for simulating natural gamma ray and density wireline logs from measurements on outcrop exposures and samples; examples from the Upper Jurassic, England, in *Core-Log Integration*, edited by P. K. Harvey, and M. A. Lovell, *Geol. Soc. Spec. Publ.*, 136, 65–80.

Algeo, T. J. (2004), Can marine anoxic events draw down the trace element inventory of seawater? *Geology*, *32*, 1057–1060, doi:10.1130/G20896.1.

Algeo, T. J., and T. W. Lyons (2006), Mo-total organic carbon covariation in modern anoxic marine environments: Implications for analysis of paleoredox and palaeohydrographic conditions, *Paleoceanography*, *21*, PA1016, doi:10.1029/2004PA001112.

Algeo, T. J., and N. Tribovillard (2009), Environmental analysis of paleoceanographic systems based on molybdenum-uranium covariation, *Chem. Geol.*, *268*, 211–225, doi:10.1016/j.chemgeo.2009.09.001.

Al-Suwaidi, A. H., G. N. Angelozzi, F. Baudin, S. E. Damborenea, S. P. Hesselbo, H. C. Jenkyns, M. O. Manceñido, and A. C. Riccardi (2010), First record of the Early Toarcian oceanic anoxic event from the Southern Hemisphere, Neuquén Basin, Argentina, *J. Geol. Soc.*, *167*, 633–636, doi:10.1144/0016-76492010-025.

Anbar, A. D. (2004), Molybdenum stable isotopes: Observations, interpretations and directions, in *Geochemistry of Non-Traditional Stable Isotopes*, edited by C. M. Johnson, B. Beard, and F. Albarède, pp. 429–454, Mineral Soc. of Am., Washington, D. C.

Archer, C., and D. Vance (2008), The isotopic signature of the global riverine molybdenum flux and anoxia in the ancient oceans, *Nat. Geosci.*, *1*, 597–600, doi:10.1038/ngeo282.

Arnold, G. L., A. D. Anbar, J. Barling, and T. W. Lyons (2004), Molybdenum isotope evidence for widespread anoxia in mid-Proterozoic oceans, *Science*, *304*, 87–90, doi:10.1126/science.1091785.

Barling, J., and A. D. Anbar (2004), Molybdenum isotope fractionation during adsorption by manganese oxides, *Earth Planet. Sci. Lett.*, *217*, 315–329, doi:10.1016/S0012-821X(03)00608-3.

Bertrand, P., and E. Lallier-Vergès (1993), Past sedimentary organic-matter accumulation and degradation controlled by productivity, *Nature*, *364*, 786–788, doi:10.1038/364786a0.

Chambers, M. H., D. S. L. Lawrence, B. W. Sellwood, and A. Parker (2000), Annual layering in the Upper Jurassic Kimmeridge Clay Formation, UK, quantified using an ultra-high resolution SEM-EDX investigation, *Sediment. Geol.*, *137*, 9–23, doi:10.1016/S0037-0738(00)00092-0.

Coe, A. L. (1992), Unconformities within the Upper Jurassic of the Wessex Basin, Southern England, Ph.D. thesis, Univ. of Oxford, Oxford, U. K.

Cohen, A. S., A. L. Coe, S. M. Harding, and L. Schwark (2004), Osmium isotope evidence for the regulation of atmospheric CO2 by continental weathering, *Geology*, *32*, 157–160, doi:10.1130/G20158.1.

Cohen, A. S., A. L. Coe, and D. B. Kemp (2007), The Late Paleocene-Early Eocene and Toarcian (Early Jurassic) carbon-isotope excursions: A comparison of their timescales, associated environmental changes, causes and consequences, *J. Geol. Soc.*, *164*, 1093–1108, doi:10.1144/0016-76492006-123.

Cope, J. C. W., T. A. Getty, M. K. Howarth, N. Morton, and H. S. Torrens (1980), A correlation of Jurassic rocks in the British Isles: Part I. Introduction to the Lower Jurassic, *Geol. Soc. Spec. Rep. 14*, pp. 1–73, Geol. Soc., London.

Cox, B. M., and R. W. Gallois (1981), The stratigraphy of the Kimmeridge Clay of the Dorset type area and its correlation with some other Kimmeridgian sequences, *Inst. Geol. Sci., Rep. No. 80/4*.

Crusius, J., and J. Thomson (2000), Comparative behavior of authigenic Re, U, and Mo during reoxidation and subsequent long-term burial in marine sediments, *Geochim. Cosmochim. Acta*, *64*, 2233–2242, doi:10.1016/S0016-7037(99)00433-0.

Crusius, J., S. Calvert, T. Pedersen, and D. Sage (1996), Rhenium and molybdenum enrichments in sediments as indicators of oxic, suboxic and sulfidic conditions of deposition, *Earth Planet. Sci. Lett.*, *145*, 65–78, doi:10.1016/S0012-821X(96)00204-X.

Demaison, G. J., and G. T. Moore (1980), Anoxic environments and oil source bed genesis, *Bull. Am. Assoc. Pet. Geol.*, *64*, 1179–1209.

Dunn, C. E. (1974), Identification of sedimentary cycles through Fourier analysis of geochemical data, *Chem. Geol.*, *13*, 217–232, doi:10.1016/0009-2541(74)90021-7.

Emerson, S. R., and S. S. Huested (1991), Ocean anoxia and the concentrations of molybdenum and vanadium in seawater, *Mar. Chem.*, *34*, 177–196, doi:10.1016/0304-4203(91)90002-E.

Glennie, K. W. (1998), *Petroleum geology of the North Sea*, 4th ed., Blackwell Sci, London, doi:10.1002/9781444313413.

Gradstein, F., J. Ogg, and A. Smith (2004), *A Geologic Time Scale*, Cambridge Univ. Press, Cambridge, U. K.

Hallam, A. (1987), Mesozoic marine organic rich shales, in *Marine Petroleum Source Rocks*, edited by J. Brooks and A. J. Fleet, *Geol. Soc. Spec. Publ.*, 26, 251–261.

Herbin, J. P., J. L. Fernandez-Martinez, J. R. Geyssant, A. El Albani, J. F. Deconinck, J. N. Proust, J. P. Colbeaux, and J. P. Vidier (1995), Sequence stratigraphy of source rocks applied to the study of the Kimmeridgian Tithonian in the north-west european shelf (Dorset/UK, Yorkshire/UK and Boulonnais/France), *Mar. Pet. Geol.*, *12*, 177–194, doi:10.1016/0264-8172(95)92838-N.

Hesselbo, S. P., D. R. Gröcke, H. C. Jenkyns, C. J. Bjerrum, P. Farrimond, H. S. Morgans-Bell, and O. R. Green (2000), Massive dissociation of gas hydrate during a Jurassic oceanic anoxic event, *Nature*, *406*, 392–395, doi:10.1038/35019044.

Hesselbo, S. P., H. C. Jenkyns, L. V. Duarte, and L. C. V. Oliveira (2007), Carbon-isotope record of the Early Jurassic (Toarcian) oceanic anoxic event from fossil wood and marine carbonate (Lusitanian Basin, Portugal), *Earth Planet. Sci. Lett.*, *253*, 455–470, doi:10.1016/j.epsl.2006.11.009.

Huang, C., S. P. Hesselbo, and L. Hinnov (2010), Astrochronology of the late Jurassic Kimmeridge Clay (Dorset, England) and implications for Earth system processes, *Earth Planet. Sci. Lett.*, *289*, 242–255, doi:10.1016/j.epsl.2009.11.013.

Jenkyns, H. C. (1985), The early Toarcian and Cenomanian-Turonian anoxic events in Europe—Comparisons and contrasts, *Geol. Rundsch.*, *74*, 505–518, doi:10.1007/BF01821208.

Jenkyns, H. C. (1988), The early Toarcian (Jurassic) anoxic event—Stratigraphic, sedimentary, and geochemical evidence, *Am. J. Sci.*, *288*, 101–151, doi:10.2475/ajs.288.2.101.

Jenkyns, H. C. (2003), Evidence for rapid climate change in the Mesozoic-Palaeogene greenhouse world, *Philos. Trans. R. Soc. London, Ser. A*, *361*, 1885–1916, doi:10.1098/rsta.2003.1240.

Jenkyns, H. C., C. E. Jones, D. Gröcke, S. P. Hesselbo, and D. Parkinson (2002), Chemostratigraphy of the Jurassic System: Applications, limitations an implications for palaeoceanography, *J. Geol. Soc.*, *159*, 351–378, doi:10.1144/0016-764901-130.

Kemp, D. B., A. L. Coe, A. S. Cohen, and L. Schwark (2005), Astronomical pacing of methane release in the Early Jurassic period, *Nature*, *437*, 396–399, doi:10.1038/nature04037.

Lallier-Vergès, E., P. Bertrand, A. Y. Huc, D. Bückel, and P. Tremblay (1993), Control of the reservation of organic matter by productivity and sulphate reduction in Kimmeridgian shales from Dorset (UK), *Mar. Pet. Geol.*, *10*, 600–605, doi:10.1016/0264-8172(93)90062-W.

Lallier-Vergès, E., J. M. Hayes, M. Boussafir, D. A. Zaback, N. P. Tribovillard, J. Connan, and P. Bertrand (1997), Productivity-induced sulphur enrichment of hydrocarbon-rich sediments from the Kimmeridge Clay Formation, *Chem. Geol.*, *134*, 277–288, doi:10.1016/S0009-2541(96)00093-9.

Lees, J. A., P. R. Bown, J. R. Young, and J. B. Riding (2004), Evidence for annual records of phytoplankton productivity in the Kimmeridge Clay Formation coccolith stone bands (Upper Jurassic, Dorset, UK), *Mar. Micropaleontol.*, *52*, 29–49, doi:10.1016/j.marmicro.2004.04.005.

Lees, J. A., P. R. Bown, and J. R. Young (2006), Photic zone palaeoenvironments of the Kimmeridge Clay Formation (Upper Jurassic, UK) suggested by calcareous nannoplankton palaeoecology, *Palaeogeogr. Palaeoclimatol. Palaeoecol.*, *235*, 110–134, doi:10.1016/j.palaeo.2005.09.026.

Ling, H. F., J. F. Gao, K. D. Zhao, S. Y. Jiang, and D. S. Mu (2005), Comment on "Molybdenum isotope evidence for widespread anoxia in mid-proterozoic oceans, *Science*, *309*, 1017c, doi:10.1126/science.1108737.

Matthews, A., H. S. Morgans-Bell, S. Emmanuel, H. C. Jenkyns, Y. Erel, and L. Halicz (2004), Controls on iron-isotope fractionation in organic-rich sediments (Kimmeridge Clay, Upper Jurassic, southern England), *Geochim. Cosmochim. Acta*, *68*, 3107–3123, doi:10.1016/j.gca.2004.01.019.

McArthur, J. M. M., T. J. Algeo, B. van de Schootbrugge, Q. Li, and R. J. Howarth (2008), Basinal restriction, black shales, Re-Os dating, and the Early Toarcian (Jurassic) oceanic anoxic event, *Paleoceanography*, *23*, PA4217, doi:10.1029/2008PA001607.

McManus, J., W. M. Berelson, S. Severmann, R. L. Poulson, D. E. Hammond, G. P. Klinkhammer, and C. Holm (2006), Molybdenum and uranium geochemistry in continental margin sediments: Paleoproxy potential, *Geochim. Cosmochim. Acta*, *70*, 4643–4662, doi:10.1016/j.gca.2006.06.1564.

Miller, R. G. (1990), A paleoceanographic approach to the Kimmeridge Clay Formation, in *Deposition of Organic Facies*, *AAPG Stud. Geol., 30*, edited by A. Y. Huc, pp. 13–26, Am. Assoc. of Pet. Geol., Tulsa, Okla.

Morford, J. L., and S. Emerson (1999), The geochemistry of redox sensitive trace metals in sediments, *Geochim. Cosmochim. Acta*, *63*, 1735–1750, doi:10.1016/S0016-7037(99)00126-X.

Morgans-Bell, H. S., A. L. Coe, S. P. Hesselbo, H. C. Jenkyns, G. P. Weedon, J. E. A. Marshall, R. V. Tyson, and C. J. Williams (2001), Integrated stratigraphy of the Kimmeridge Clay Formation (Upper Jurassic) based on exposures and boreholes in south Dorset, UK, *Geol. Mag.*, *138*, 511–539, doi:10.1017/S0016756801005738.

Neubert, N., T. F. Nägler, and M. E. Böttcher (2008), Sulfidity controls molybdenum isotope fractionation into euxinic sediments: Evidence from the modern Black Sea, *Geology*, *36*, 775–778, doi:10.1130/G24959A.1.

Oschmann, W. (1988), Kimmeridge Clay sedimentation—A new cyclic model, *Palaeogeogr. Palaeoclimatol. Palaeoecol.*, *65*, 217–251, doi:10.1016/0031-0182(88)90025-9.

Oschmann, W. (1990), Environmental cycles in the Late Jurassic Northwest European epeiric basin—Interaction with atmospheric and hydrospheric circulations, *Sediment. Geol.*, *69*, 313–332, doi:10.1016/0037-0738(90)90056-Y.

Padden, M., H. Weissert, H. Funk, S. Schneider, and C. Gansner (2002), Late Jurassic lithological evolution and carbon-isotope stratigraphy of the western Tethys, *Eclogae Geol. Helv.*, *95*, 333–346.

Pálfy, J., and P. L. Smith (2000), Synchrony between Early Jurassic extinction, oceanic anoxic event, and the Karoo-Ferrar flood basalt volcanism, *Geology*, *28*, 747–750, doi:10.1130/0091-7613(2000)28<747:SBEJEO>2.0.CO;2.

Pearce, C. R., A. S. Cohen, A. L. Coe, and K. W. Burton (2008), Molybdenum isotope evidence for global ocean anoxia coupled with perturbations to the carbon cycle during the Early Jurassic, *Geology*, *36*, 231–234, doi:10.1130/G24446A.1.

Pearce, C. R., A. S. Cohen, and I. J. Parkinson (2009), Quantitative separation of molybdenum and rhenium from geological materials for isotopic analysis by MC-ICP-MS, *Geostand. Geoanal. Res.*, *33*, 219–229, doi:10.1111/j.1751-908X.2009.00012.x.

Pearson, S. J., J. E. A. Marshall, and A. E. S. Kemp (2004), The white stone band of the Kimmeridge Clay formation, an integrated high-resolution approach to understanding environmental change, *J. Geol. Soc.*, *161*, 675–683, doi:10.1144/0016-764903-089.

Piper, D. Z., and S. E. Calvert (2009), A marine biogeochemical perspective on black shale deposition, *Earth Sci. Rev.*, *95*, 63–96, doi:10.1016/j.earscirev.2009.03.001.

Poulson, R., C. Siebert, J. McManus, and W. M. Berelson (2006), Authigenic molybdenum isotope signatures in marine sediments, *Geology*, *34*, 617–620, doi:10.1130/G22485.1.

Raiswell, R., and R. A. Berner (1985), Pyrite formation in euxinic and semieuxinic sediments, *Am. J. Sci.*, *285*, 710–724, doi:10.2475/ajs.285.8.710.

Raiswell, R., F. Buckley, R. A. Berner, and T. F. Anderson (1988), Degree of pyritization of iron as a paleoenvironmental indicator of bottom-water oxygenation, *J. Sediment. Petrol.*, *58*, 812–819.

Sælen, G., R. V. Tyson, N. Telnaes, and M. R. Talbot (2000), Contrasting water mass conditions during deposition of the Whitby Mudstone (Lower Jurassic) and Kimmeridge Clay (Upper Jurassic) formations, UK, *Palaeogeogr. Palaeoclimatol. Palaeoecol.*, *163*, 163–196, doi:10.1016/S0031-0182(00)00150-4.

Schouten, S., H. M. E. van Kaam Peters, W. I. C. Rijpstra, M. Schoell, and J. S. Sinninghe Damsté (2000), Effects of an oceanic anoxic event on the stable carbon isotopic composition of Early Toarcian carbon, *Am. J. Sci.*, *300*, 1–22, doi:10.2475/ajs.300.1.1.

Siebert, C., T. F. Nägler, F. von Blanckenburg, and J. D. Kramers (2003), Molybdenum isotope records as a potential new proxy for paleoceanography, *Earth Planet. Sci. Lett.*, *211*, 159–171, doi:10.1016/S0012-821X(03)00189-4.

Siebert, C., J. McManus, A. Bice, R. Poulson, and W. M. Berelson (2006), Molybdenum isotope signatures in continental margin marine sediments, *Earth Planet. Sci. Lett.*, *241*, 723–733, doi:10.1016/j.epsl.2005.11.010.

Sinninghe Damsté, J. S., S. Schouten, and A. Van Duin (2001), Isorenieratene derivatives in sediments: Possible controls on their distribution, *Geochim. Cosmochim. Acta*, *65*, 1557–1571, doi:10.1016/S0016-7037(01)00549-X.

Smith, A. G., D. G. Smith, and B. Funnell (1994), Atlas of Mesozoic and Cenozoic Coastlines, Cambridge Univ. Press, Cambridge.

Taylor, S. P., B. W. Sellwood, R. W. Gallois, and M. H. Chambers (2001), A sequence stratigraphy of the Kimmeridgian and Bolonian stages (late Jurassic): Wessex-Weald Basin, southern England, *J. Geol. Soc.*, *158*, 179–192, doi:10.1144/jgs.158.1.179.

Tossell, J. A. (2005), Calculating the partitioning of the isotopes of Mo between oxidic and sulfidic species in aqueous solution, *Geochim. Cosmochim. Acta*, *69*, 2981–2993, doi:10.1016/j.gca.2005.01.016.

Tribovillard, N., A. Despraires, E. Lallier-Vergès, N. Moureau, A. Ramdani, and L. Ramanampisoa (1994), Geochemical study of organic-matter rich cycles from the Kimmeridge Clay Formation of Yorkshire (UK)—Productivity vs. anoxia, *Palaeogeogr. Palaeoclimatol. Palaeoecol.*, *108*, 165–181, doi:10.1016/0031-0182(94)90028-0.

Tribovillard, N., A. Riboulleau, T. Lyons, and F. O. Baudin (2004a), Enhanced trapping of molybdenum by sulfurized marine organic matter of marine origin in Mesozoic limestones and shales, *Chem. Geol.*, *213*, 385–401, doi:10.1016/j.chemgeo.2004.08.011.

Tribovillard, N., A. Trentesaux, A. Ramdani, F. Baudin, and A. Riboulleau (2004b), Controls on organic accumulation in late Jurassic shales of northwestern Europe as inferred from trace metal geochemistry, *Bull. Soc. Geol. Fr.*, *175*, 491–506, doi:10.2113/175.5.491.

Tribovillard, N., T. J. Algeo, T. Lyons, and A. Riboulleau (2006), Trace metals as paleoredox and paleoproductivity proxies: An update, *Chem. Geol.*, *232*, 12–32, doi:10.1016/j.chemgeo.2006.02.012.

Tyson, R. V. (1979), Environmental-model for the type Kimmeridge Clay—Reply, *Nature*, *279*, 819–820, doi:10.1038/279819b0.

Tyson, R. V. (2004), Variation in marine total organic carbon through the type Kimmeridge Clay Formation (Late Jurassic), Dorset, UK, *J. Geol. Soc.*, *161*, 667–673, doi:10.1144/0016-764903-078.

Tyson, R. V. (2005), The productivity versus preservation controversy: Cause, flaws, and resolution, *SEPM Spec. Publ.*, *82*, 17–33.

van Dongen, B. E., S. Schouten, and J. S. Sinninghe Damsté (2006), Preservation of carbohydrates through sulfurization in a Jurassic euxinic shelf sea: Examination of the Blackstone Band TOC cycle in the Kimmeridge Clay Formation, UK, *Org. Geochem.*, *37*, 1052–1073, doi:10.1016/j.orggeochem.2006.05.007.

van Kaam-Peters, H. M. E., W. I. C. Rijpstra, J. W. de Leeuw, and J. S. Sinninghe Damsté (1998a), A high resolution biomarker study of different lithofacies of organic sulfur-rich carbonate rocks of a Kimmeridgian lagoon (French southern Jura), *Org. Geochem.*, *28*, 151–177, doi:10.1016/S0146-6380(97)00132-0.

van Kaam-Peters, H. M. E., S. Schouten, J. Koster, and J. S. Sinninghe Damsté (1998b), Controls on the molecular and carbon isotopic composition of organic matter deposited in a Kimmeridgian euxinic shelf sea: Evidence for preservation of carbohydrates through sulfurisation, *Geochim. Cosmochim.*

Acta, *62*, 3259–3283, doi:10.1016/S0016-7037(98)00231-2.

Weedon, G. P., H. C. Jenkyns, A. L. Coe, and S. P. Hesselbo (1999), Astronomical calibration of the Jurassic time-scale from cyclostratigraphy in British mudrock formations, *Philos. Trans. R. Soc. London, Ser. A*, *357*, 1787–1813, doi:10.1098/rsta.1999.0401.

Weedon, G. P., A. L. Coe, and R. W. Gallois (2004), Cyclostratigraphy, orbital tuning and inferred productivity for the type Kimmeridge Clay (Late Jurassic), Southern England, *J. Geol. Soc.*, *161*, 655–666, doi:10.1144/0016-764903-073.

Weissert, H., and H. Mohr (1996), Late Jurassic climate and its impact on carbon cycling, *Palaeogeogr. Palaeoclimatol. Palaeoecol.*, *122*, 27–43, doi:10.1016/0031-0182(95)00088-7.

Wignall, P. B., and K. J. Meyers (1988), Interpreting benthic oxygen levels in mudrocks: A new approach, *Geology*, *16*, 452–455, doi:10.1130/0091-7613(1988)016<0452:IBOLIM>2.3.CO;2.

Wignall, P. B., and R. Newton (2001), Black shales on the basin margin: A model based on examples from the Upper Jurassic of the Boulonnais, northern France, *Sediment. Geol.*, *144*, 335–356, doi:10.1016/S0037-0738(01)00125-7.

Wignall, P. B., and A. H. Ruffell (1990), The Influence of a sudden climatic-change on marine deposition in the Kimmeridgian of Northwest Europe, *J. Geol. Soc.*, *147*, 365–371, doi:10.1144/gsjgs.147.2.0365.

Ziegler, P. (1990), *Geological Atlas of Western and Central Europe*, 2nd ed., Shell Intl. Pet. Maatschappij B.V, Netherlands.

A. L. Coe, A. S. Cohen, and C. R. Pearce, Department of Earth and Environmental Sciences, Centre for Earth, Planetary, Space and Astronomical Research, Open University, Walton Hall, Milton Keynes MK7 6AA, UK. (c.pearce@open.ac.uk)